

Ray model of light scattering by flake pigments or rough surfaces with smooth transparent coatings

Thomas A. Germer and Egon Marx
National Institute of Standards and Technology
Gaithersburg, Maryland 20899

We derive expressions for the intensity and polarization of light singly scattered by flake pigments or a rough surface beneath a smooth transparent coating using the ray or facet model. The distribution of local surface normals is used to calculate the bidirectional reflectance distribution function (BRDF). We discuss the different distribution functions that can be used to characterize the distribution of local surface normals. The light scattering model is validated using measurements of the BRDF and polarization by a metallic flake pigmented coating. The results enable the extraction of a slope distribution function from the data, which is shown to be consistent over a variety of scattering geometries. These models are appropriate for estimating or predicting the appearance of flake pigment automotive paints.

OCIS Codes: 030.5770, 080.2720, 120.5820, 290.5880

1. Introduction

The scattering of light by special-effect flake pigments in smooth transparent coatings strongly affects the appearance of automotive coatings.^{1,2} Predicting and visualizing the appearance of coatings before they are manufactured helps to reduce the cost of developing new products. Having models for light scattering aids in the virtual design of these coatings. They improve quality control, both by enabling estimates of parameter tolerances, and by providing scaling properties that reduce the number of measurements that are required to accurately characterize the coatings.

The flake pigments used in many automotive coatings consist of platelets of metal or dielectric material, with face dimensions ranging from a few micrometers to a couple hundred micrometers and thicknesses ranging from tens of nanometers to hundreds of nanometers.¹ These flakes can have interference coatings applied to them to give them more distinctive appearance properties. They are generally embedded in a transparent binder, and a final coating, with an optically-similar material as the binder, is applied to provide a smooth, glossy finish.

In this paper, we present and validate the derivation of procedures used to compute the bidirectional reflectance distribution function^{3,4} (BRDF) for flake pigment coatings and rough surfaces covered by a dielectric coating. The derivation in Sec. 2 provides an extension to theories developed in the past for scattering by rough surfaces without a coating.⁵⁻⁷ In Sec. 3, we describe measurements that we performed to test the validity of the model. Theoretical and experimental results are presented in Sec. 4. Finally, we conclude with remarks in Sec. 5.

2. Theory

The derivation of the BRDF for flakes or a rough surface beneath a smooth coating is divided into five subsections. In Sec. 2.A, we present an overview of the model and the approximations made. In Sec. 2.B, we derive the net reflectance of a tilted surface facet beneath a coating material. We then discuss in Sec. 2.C the various distribution functions that can be used to characterize the orientations of the surface facets. Next, in Sec. 2.D, we calculate the probability that a ray will reflect from a specific incident direction to a specific viewing direction. Finally, In Sec. 2.E, we summarize the theoretical discussion by combining the results to give expressions for the BRDF.

2.A. Description of the model

A flake pigment embedded in a paint coating can be characterized by a probability distribution for the position, orientation, and properties of the flakes contained in a dielectric layer of uniform thickness. If the flakes are flat, large compared to the wavelength, and sparse enough so that we can neglect multiple scattering or shadowing, it is sufficient to give the distribution of the normals of the flakes, weighted by their area, which determine the direction of a light ray reflected by the flake. The distribution in a particular coating can, for instance, be directly determined from data collected with a confocal microscope.⁸ We consider a coating that contains no pigments other than the flakes, which can be dielectric or can have finite conductivity.

A random rough surface can be characterized by probability distributions for the height or slope. If the features on the surface are large compared to the wavelength of the incident light, it can be considered locally flat and the scattered light is determined by specular reflection from surface facets. An instance of a random rough surface can be furnished by a topographic map obtained with an interferometric microscope.⁹ The rough surface can be considered as a collection of facets, which correspond to flakes that cover the surface and leave no interstices.

We treat the interface between the ambient medium (air or vacuum) and the coating to be flat with no roughness. The coating is non-absorbing with an index of refraction n . Beneath the coating is a rough interface to an optically thick substrate material, or embedded within the coating are flat platelets or flakes. The material of the flakes, or under the rough interface, has a complex index of refraction n_f .

Let the rough surface or the outwardly directed faces of the flakes consist of a surface having a single-valued height (z coordinate) for each point (x,y) on the rough surface or on a flake. If this surface can be broken up into locally flat surface elements (facets) in such a manner that the surface elements are much greater in dimension than the wavelength of the light in the coating, and if there exists no correlation amongst different surface elements, then we can treat the scattering in the physical optics, or ray, approximation. Figure 1 shows the propagation of a ray which specularly reflects from a specific oblique surface element. In the case of flakes, this surface element can be an entire flake, if the flake is sufficiently flat, or it can represent a small part of a rough flake. The surface elements do not have to be connected.

In that approximation, a ray incident upon the material will transmit into the coating, reflect from a random surface element whose orientation is determined by some distribution, and then transmit out of the coating. The bidirectional reflectance distribution function f_r is thus related to the product of the probability $P(\theta_i, \theta_r, \phi_r) d\Omega_r$ that a ray will reflect from a direction

defined by angle θ_i to a direction defined by polar angle θ_r and ϕ_r , and the net reflectance R_{net} of the path:

$$f_r(\theta_i, \theta_r, \phi_r) = P(\theta_i, \theta_r, \phi_r) R_{\text{net}} / \cos \theta_r. \quad (1)$$

We let the incident azimuthal angle be $\phi_i = \pi$.

In our model, we make a number of further simplifying assumptions and approximations. We choose to ignore multiply scattered light. Light which is reflected by the coating interface after having been reflected by a surface element may interact with other surface elements. If the surface elements are highly reflective, then ignoring this contribution to the scattered light can potentially lead to large errors. Furthermore, for flakes which transmit a significant fraction of the light incident upon them, interaction with flakes beneath others will occur. We also assume that the surface elements do not shadow or obscure other surface elements. This means that the surface cannot be too rough, or if there are flakes, that the flakes do not significantly obscure other flakes, making them inaccessible to the incident light.

We can determine the relationship between the scattering geometry and the orientation of the facet which specularly reflects in that geometry, shown in Fig. 1. Angles of rays within the coating are related to angles outside the coating by Snell's law:

$$n \sin \theta'_i = \sin \theta_i, \quad (2)$$

$$n \sin \theta'_r = \sin \theta_r, \quad (3)$$

$$\phi'_r = \phi_r. \quad (4)$$

The requirement that light propagating at angle θ'_i specularly reflects into a direction defined by polar angles θ'_r and ϕ'_r leads to a unique orientation for the surface facet. The cosine of the local angle of incidence onto the facet is given by

$$\cos \alpha = [(1 - \sin \theta'_i \sin \theta'_r \cos \phi_r + \cos \theta'_i \cos \theta'_r) / 2]^{1/2}, \quad (5)$$

and the cosine of the polar angle of the facet normal is given by

$$\cos \theta_n = (\cos \theta'_i + \cos \theta'_r) / (2 \cos \alpha). \quad (6)$$

The azimuthal angle of the facet normal can be determined from

$$\phi'_n = \arctan(\cos \theta'_r \cos \phi'_r - \cos \theta'_i, \cos \theta'_r \sin \phi'_r), \quad (7)$$

where the two-argument $\arctan(a,b)$ returns the arctangent of b/a , taking into account the quadrant where (a,b) lies.

2.B. Net reflectance of a ray upon a surface facet

We evaluate the net reflectance R_{net} for the ray shown in Fig. 1. R_{net} depends upon the transmittance of the ray into the coating, the reflectance from the surface element, and the

subsequent transmittance of the ray out of the coating. Each of these values depends upon the incident polarization and measurement of the scattered polarization. We begin by defining orthogonal basis vectors by which the polarization states are defined. Unprimed unit vectors represent those basis vectors which are most natural to rays external to the material, primed unit vectors represent those basis vectors which are most natural for rays in the overcoat, and subscripts i and r represent rays before and after reflection from the facet, respectively. The basis vectors are chosen so that $\{\hat{\mathbf{s}}, \hat{\mathbf{p}}, \hat{\mathbf{k}}\}$ form a right-handed set of vectors, with $\hat{\mathbf{k}}$ being a unit vector in the direction of propagation, $\hat{\mathbf{s}}$ being a unit vector parallel to the xy plane, and $\hat{\mathbf{p}}$ being parallel to the plane defined by the z direction and $\hat{\mathbf{k}}$. For example, the scattered light polarization unit vectors are

$$\hat{\mathbf{s}}_r = -\hat{\mathbf{x}} \cos \phi_r + \hat{\mathbf{y}} \cos \phi_r, \quad (8a)$$

$$\hat{\mathbf{p}}_r = \hat{\mathbf{x}} \cos \theta_r \cos \phi_r + \hat{\mathbf{y}} \cos \theta_r \sin \phi_r + \hat{\mathbf{z}} \sin \theta_r. \quad (8b)$$

Dyadics relate incident electric fields to reflected or transmitted electric fields. For example, the relationship between the electric field amplitude incident upon the coating interface, $\hat{\mathbf{E}}_i$, and the electric field amplitude transmitted into the coating, \mathbf{E}'_i , is given by

$$\mathbf{E}'_i = \vec{\mathbf{t}}_i(\theta_i; 1, n) \cdot \mathbf{E}_i, \quad (9)$$

where

$$\vec{\mathbf{t}}_i(\theta_i; 1, n) = t_s(\theta_i; 1, n) \hat{\mathbf{s}}_i \hat{\mathbf{s}}_i + t_p(\theta_i; 1, n) \hat{\mathbf{p}}_i \hat{\mathbf{p}}_i, \quad (10)$$

and $t_{s,p}(\theta; n_1, n_2)$ is the Fresnel transmission coefficient for s,p-polarized light when the incident angle is θ , the refractive index of the incident medium is n_1 , and that of the transmitting medium is n_2 . For a single interface, expressions for the Fresnel coefficients are given in the Appendix. More complicated expressions can be determined if the boundary between the materials contains interference coatings.¹⁰ The dyadic relating the electric field amplitudes before and after reflection from the surface facet element is given by

$$\vec{\mathbf{r}}(\alpha; n, n_f) = r_s(\alpha; n, n_f) \hat{\mathbf{s}}'_i \hat{\mathbf{s}}'_i + r_p(\alpha; n, n_f) \hat{\mathbf{p}}'_i \hat{\mathbf{p}}'_i, \quad (11)$$

where $r_{s,p}(\theta; n_1, n_2)$ is the Fresnel reflection coefficient for s,p-polarized light when the incident angle is θ , the incident medium is n_1 , and the transmitting medium is n_2 . The dyadic relating the electric field amplitudes on the two sides of the coating for light exiting the coating is given by

$$\vec{\mathbf{t}}_r(\theta'_r; n, 1) = t_s(\theta'_r; n, 1) \hat{\mathbf{s}}_r \hat{\mathbf{s}}_r + t_p(\theta'_r; n, 1) \hat{\mathbf{p}}_r \hat{\mathbf{p}}_r, \quad (12)$$

The net dyadic relating the incident electric field amplitude to that leaving the system is given by

$$\hat{\mathbf{r}}_{\text{net}} = \vec{\mathbf{t}}_r(\theta'_r; n, 1) \cdot \vec{\mathbf{r}}(\alpha; n, n_f) \cdot \vec{\mathbf{t}}_i(\theta_i; 1, n), \quad (13)$$

where we ignore the overall phase due to the propagation between events. In order to make the final result appear more symmetric with respect to interchange of incident and scattering directions, we use the identity

$$t_{s,p}(\theta'_r; n, 1) = \frac{n \cos \theta'_r}{\cos \theta_r} t_{s,p}(\theta_r; 1, n) \quad (14)$$

to write Eq. (12) as

$$\vec{\mathbf{t}}_r(\theta'_r; n, 1) = \frac{n \cos \theta'_r}{\cos \theta_r} [t_s(\theta_r; 1, n) \hat{\mathbf{s}}_r \hat{\mathbf{s}}'_r + t_p(\theta_r; 1, n) \hat{\mathbf{p}}_r \hat{\mathbf{p}}'_r]. \quad (15)$$

The net dyadic in Eq. (13) can then be written in the form

$$\vec{\mathbf{r}}_{\text{net}} = \frac{n \cos \theta'_r}{\cos \theta_r} \vec{\mathbf{q}} \quad (16)$$

Combining Eqs. (10), (11), (13), (15) and (16), using unit vectors like those in Eqs. (8), the dyadic $\vec{\mathbf{q}}$ can be written as

$$\vec{\mathbf{q}} = q_{ss} \hat{\mathbf{s}}_r \hat{\mathbf{s}}_i + q_{sp} \hat{\mathbf{s}}_r \hat{\mathbf{p}}_i + q_{ps} \hat{\mathbf{p}}_r \hat{\mathbf{s}}_i + q_{pp} \hat{\mathbf{p}}_r \hat{\mathbf{p}}_i \quad (17)$$

where

$$q_{ss} = t_s(\theta_i; 1, n) t_s(\theta_r; 1, n) [r_p(\alpha; n, n_f) \sin \theta'_i \sin \theta'_r \sin^2 \phi_r + a_2 a_3 r_s(\alpha; n, n_f)] / a_1 \quad (18a)$$

$$q_{ps} = -t_s(\theta_i; 1, n) t_p(\theta_r; 1, n) \sin \phi_r [a_2 r_s(\alpha; n, n_f) \sin \theta'_r - a_3 r_p(\alpha; n, n_f) \sin \theta'_i] / a_1 \quad (18b)$$

$$q_{sp} = -t_p(\theta_i; 1, n) t_s(\theta_r; 1, n) \sin \phi_r [a_3 r_s(\alpha; n, n_f) \sin \theta'_i - a_2 r_p(\alpha; n, n_f) \sin \theta'_r] / a_1 \quad (18c)$$

$$q_{pp} = t_p(\theta_i; 1, n) t_p(\theta_r; 1, n) [r_s(\alpha; n, n_f) \sin \theta'_i \sin \theta'_r \sin^2 \phi_r + a_2 a_3 r_p(\alpha; n, n_f)] / a_1 \quad (18d)$$

and

$$a_1 = \sin^2 2\alpha \quad (19a)$$

$$a_2 = \cos \theta'_i \sin \theta'_r + \sin \theta'_i \cos \theta'_r \cos \phi_r \quad (19b)$$

$$a_3 = \sin \theta'_i \cos \theta'_r + \cos \theta'_i \sin \theta'_r \cos \phi_r. \quad (19c)$$

To calculate the reflectance, we note that energy conservation is expressed as a balance of the power flowing in a direction perpendicular to the surface, which is proportional to the products of the Poynting vector and the cosine of the angle between the propagation vector and the normal. The net energy reflectance is thus given by

$$R_{\text{net}} = \frac{\cos \theta'_i \cos \theta_r}{\cos \theta_i \cos \theta'_r} |\vec{\mathbf{r}}_{\text{net}} \cdot \mathbf{E}_i|^2 = \frac{n^2 \cos \theta'_i \cos \theta'_r}{\cos \theta_i \cos \theta_r} |\vec{\mathbf{q}} \cdot \mathbf{E}_i|^2 \quad (20)$$

The net reflectance given in Eq. (20), expressed in terms of the dyadic $\vec{\mathbf{q}}$, can be seen to be symmetric upon interchange of incident and scattering direction.

2.C. Descriptions of the facet orientation statistics

The distribution of local surface normals \hat{n} can be quantified in a number of different ways. For example, we can characterize it by the distribution of the angles the surface normal makes with the z direction, θ_n and ϕ_n , and speak of the probability that the orientation is within a specific solid angle $d\Omega_n = \sin \theta_n d\theta_n d\phi_n$ about this direction. Alternatively, we can characterize the surface normals with respect to their directional slope ζ_x and ζ_y , and consider the probability that the directional slope is with a differential slope element $d\zeta_x d\zeta_y$, where the slopes are related to the polar angles by

$$\zeta_x = \tan \theta_n \cos \phi_n, \quad (21a)$$

$$\zeta_y = \tan \theta_n \sin \phi_n. \quad (21b)$$

For azimuthally isotropic distributions, we can also characterize the orientation distributions in terms of single variables, for example, the probability that the angle θ_n is between θ_n and $\theta_n + d\theta_n$ or that the slope $\zeta = (\zeta_x^2 + \zeta_y^2)^{1/2}$ is between ζ and $\zeta + d\zeta$. Quantification of the orientation distribution is further complicated by the need to chose whether points on the surface are to be chosen uniformly on the mean surface plane, or whether they are to be chosen uniformly on the actual surface. It is convenient to characterize rough surfaces by a slope distribution function choosing points on the mean surface plane, while it is more convenient to characterize flake pigments by an angle distribution using the points chosen on the actual flakes. In the following, we will relate these probability densities to each other. We will affix a superscript xy or A to signify if the sampling is performed uniformly on the mean surface plane or on the actual surface, respectively.

We define the probability that the surface normal has angles θ_n and ϕ_n within a specific solid angle $d\Omega_n = \sin \theta_n d\theta_n d\phi_n$ of the direction defined by θ_n and ϕ_n , sampling uniformly on the mean surface plane, to be

$$P_1^{xy}(\theta_n, \phi_n) d\Omega_n. \quad (22)$$

The probability that the angle θ_n is between θ_n and $\theta_n + d\theta_n$ is given by

$$P_2^{xy}(\theta_n) d\theta_n = \int P_1^{xy}(\theta_n, \phi_n) \sin \theta_n d\phi_n d\theta_n. \quad (23)$$

If $P_1^{xy}(\theta_n, \phi_n)$ does not depend upon ϕ_n , we can relate it to $P_2^{xy}(\theta_n)$:

$$P_2^{xy}(\theta_n) d\theta_n = 2\pi P_1^{xy}(\theta_n, 0) \sin \theta_n d\theta_n. \quad (24)$$

The probability that the directional slope is within $d\zeta_x d\zeta_y$ of (ζ_x, ζ_y) will be defined as

$$P_3^{xy}(\zeta_x, \zeta_y) d\zeta_x d\zeta_y. \quad (25)$$

Likewise, the probability that $\zeta = (\zeta_x^2 + \zeta_y^2)^{1/2}$ is between ζ and $\zeta + d\zeta$ is given by

$$P_4^{xy}(\zeta) d\zeta = \int P_3^{xy}(\zeta_x, \zeta_y) \zeta d\phi_n d\zeta. \quad (26)$$

Again, for an azimuthally isotropic distribution,

$$P_4^{xy}(\zeta) d\zeta = 2\pi \zeta P_3^{xy}(\zeta, 0) d\zeta. \quad (27)$$

The relationship between $P_1^{xy}(\theta_n, \phi_n)$ and $P_3^{xy}(\zeta_x, \zeta_y)$ requires the Jacobian

$$\frac{\partial(\zeta_x, \zeta_y)}{\partial(\theta_n, \phi_n)} = \sin \theta_n \sec^3 \theta_n, \quad (28)$$

so that

$$P_3^{xy}(\zeta_x, \zeta_y) = \cos^3 \theta_n P_1^{xy}(\theta_n, \phi_n), \quad (29)$$

and, for an isotropic distribution,

$$P_4^{xy}(\zeta) = \cos^2 \theta_n P_2^{xy}(\theta_n). \quad (30)$$

Since the probability of finding a flake, sampling the surface uniformly on the mean surface plane is the coverage of the facets projected onto the xy plane, C , we expect the normalizations

$$\int P_1^{xy}(\theta_n, \phi_n) \sin \theta_n d\theta_n d\phi_n = C, \quad (31)$$

$$\int P_2^{xy}(\theta_n) d\theta_n = C, \quad (32)$$

$$\int P_3^{xy}(\zeta_x, \zeta_y) d\zeta_x d\zeta_y = C, \quad (33)$$

$$\int P_4^{xy}(\zeta) d\zeta = C. \quad (34)$$

For a continuous rough surface, $C = 1$.

The distributions above were given for points uniformly sampled on the mean surface plane. Orientation distributions for points sampled uniformly on the actual surface elements can be defined, too, analogously to Eqs. (22)–(30): $P_1^A(\theta_n, \phi_n)$, $P_2^A(\theta_n)$, $P_3^A(\zeta_x, \zeta_y)$, and $P_4^A(\zeta)$.

Since the projection of the area of a facet on the mean surface plane is proportional to $\cos \theta_n$, the probability distribution

$$P_1^A(\theta_n, \phi_n) = \sec \theta_n P_1^{xy}(\theta_n, \phi_n) / (C \langle \sec \theta_n \rangle), \quad (35)$$

where the average of $\sec \theta_n$ is that sampled over the mean surface plane which is covered and is included to guarantee that $P_1^A(\theta_n, \phi_n)$ is properly normalized. Given explicitly,

$$\langle \sec \theta_n \rangle = \frac{1}{C} \int \sec \theta_n P_1^{xy}(\theta_n, \phi_n) \sin \theta_n d\theta_n d\phi_n. \quad (36)$$

The normalizations are thus

$$\int P_1^A(\theta_n, \phi_n) \sin \theta_n d\theta_n d\phi_n = 1, \quad (37)$$

$$\int P_2^A(\theta_n) d\theta_n = 1, \quad (38)$$

$$\int P_3^A(\zeta_x, \zeta_y) d\zeta_x d\zeta_y = 1, \quad (39)$$

$$\int P_4^A(\zeta) d\zeta = 1. \quad (40)$$

The relationship between $P_1^A(\theta_n, \phi_n)$ and $P_3^{xy}(\zeta_x, \zeta_y)$ can be determined from Eqs. (29) and (35):

$$P_1^A(\theta_n, \phi_n) = \sec^4 \theta_n P_3^{xy}(\zeta_x, \zeta_y) / (C \langle \sec \theta_n \rangle) \quad (41)$$

The distributions can be parameterized by any of a number of functions. There is no clear preferred choice of one over another, and one can choose which distribution to parameterize. In this article, we will use an exponential slope distribution function,

$$P_3^{xy}(\zeta_x, \zeta_y) = \frac{3A}{\pi\sigma^2} \exp(-\sqrt{6}\zeta / \sigma), \quad (42)$$

where σ is the root-mean-square of the surface slope. Eq. (42) is normalized to obey Eq. (33).

2.D. The ray direction probability

In this section, we will calculate the probability $P(\theta_r, \theta_r, \phi_r) d\Omega_r$ that a ray incident at an angle θ_i will result in a ray directed within a solid angle $d\Omega_r$ about the direction defined by polar angles θ_r and ϕ_r . We can begin by using any of the two-variable probability distributions described above, being able to convert our result to any of the others by using the relationships between them. We choose the probability density $P_1^{xy}(\theta_n, \phi_n)$, since it is the easiest from which to start. A facet having an orientation (θ_n, ϕ_n) which has a projected area dA on the xy plane will have an area $dA / \cos \theta_n$, and will have a projected area $\cos \alpha dA / \cos \theta_n$ onto a plane perpendicular to the incident direction in the coating. If the total area of the xy plane illuminated by the incident beam is A , then the cross sectional area of the incident beam in the coating is $A \cos \theta_i'$. Assuming that there is no shadowing of surface facets, the probability that a ray propagating in the coating will strike a facet of orientation (θ_n, ϕ_n) within a solid angle $d\Omega_n$ is thus given by

$$P_1^{xy}(\theta_n, \phi_n) \cos \alpha d\Omega_n / (\cos \theta_n \cos \theta_i'). \quad (43)$$

Eq. (43) is the probability for striking a flake whose normal is within a solid angle $d\Omega_n$. Since we need the probability for reflecting into solid angle $d\Omega_r$, we need to determine the ratio $d\Omega_r / d\Omega_n$. From Snell's law, we calculate the Jacobian

$$\partial(\theta_r, \phi_r) / \partial(\theta_r', \phi_r') = n \cos \theta_r' / \cos \theta_r. \quad (44)$$

From Eq. (6), we calculate the Jacobian

$$\partial(\theta_r', \phi_r') / \partial(\theta_n, \phi_n) = 4(\sin \theta_n / \sin \theta_r') \cos \alpha. \quad (45)$$

Combining Eqs. (44) and (45), we have

$$d\Omega_r / d\Omega_n = (\sin \theta_r / \sin \theta_n) \partial(\theta_r, \phi_r) / \partial(\theta_n, \phi_n) = 4n^2 \cos \theta_r' \cos \alpha / \cos \theta_r. \quad (46)$$

Finally, by combining Eqs. (43) and (46), we arrive at the probability of an incident ray striking a flake which reflects the light into a solid angle $d\Omega_r$ about direction (θ_r, ϕ_r) :

$$P(\theta_i, \theta_r, \phi_r) d\Omega_r = P_1^{xy}(\theta_n, \phi_n) \cos \theta_r d\Omega_r / (4n^2 \cos \theta'_r \cos \theta'_i \cos \theta_n). \quad (47)$$

2.E. The BRDF for flakes and rough surfaces

The BRDF is found by combining Eqs. (1), (20), and (47):

$$f_r = \frac{P_1^{xy}(\theta_n, \phi_n)}{4 \cos \theta_i \cos \theta_r \cos \theta_n} |\vec{\mathbf{q}} \cdot \mathbf{E}_i|^2. \quad (48)$$

If one wishes to express the BRDF with respect to the slope distribution function evaluated for points sampled uniformly on the mean surface plane, then we can combine Eq. (29) with Eq. (48):

$$f_r = \frac{P_3^{xy}(\zeta_x, \zeta_y)}{4 \cos \theta_i \cos \theta_r \cos^4 \theta_n} |\vec{\mathbf{q}} \cdot \mathbf{E}_i|^2. \quad (49)$$

Likewise, if one wishes to express the BRDF with respect to the angle distribution function evaluated for points sampled uniformly on the faceted surface, then we can apply Eq. (41) to Eq. (49):

$$f_r = \frac{C \langle \sec \theta_n \rangle P_1^A(\theta_n, \phi_n)}{4 \cos \theta_i \cos \theta_r} |\vec{\mathbf{q}} \cdot \mathbf{E}_i|^2 \quad (50)$$

It can be seen that Eqs. (48)–(50) follow Helmholtz reciprocity by being symmetric upon interchange of incident and scattering directions.

3. Experiment

Measurements were performed using the Goniometric Optical Scatter Instrument,^{11,12} a laser-based system having a high angular resolution, wide dynamic range, full polarimetric capabilities, and the ability to measure scattering out of the plane of incidence. Measurements performed for this study used a HeNe laser ($\lambda = 632.8$ nm) and were carried out in two different geometry-scanning modes: in-plane and out-of-plane. In-plane measurements were carried out with fixed incident angle ($\theta_i = 45^\circ$ and 60°), scanning the scattering angle in the plane of incidence. Out-of-plane measurements were carried out by fixing the incident and scattering polar angles ($\theta_i = \theta_r = 45^\circ$ and 60°), while scanning the azimuthal scattering angle ϕ_r from 0° (specular direction) to near 180° (the retroreflection direction). Measurements of the Stokes vector BRDF were performed, using specific incident polarizations which yield a high degree of discrimination between scattering sources. In the plane of incidence, such discrimination was obtained by letting the incident light be linearly polarized at 45° to the plane of incidence. For out-of-plane measurements, the incident polarization was continuously varied from 45° (p+s) at $\phi_r = 0^\circ$, to 90° (p) at $\phi_r = 90^\circ$, and to 135° (p-s) at $\phi_r = 180^\circ$. This incident polarization scheme

improves the discrimination between the different scattering mechanisms for all ϕ_r , compared to the discrimination found using a fixed incident polarization state.¹³

The intensity and polarization of the scattered light is characterized by the BRDF, f_r , the principal angle of the polarization, η (measured counterclockwise from s-polarization when viewing into the direction of propagation), the degree of circular polarization, P_C , and the total degree of polarization, P . The sign of P_C is chosen to be positive for left-circularly polarized light. These parameters can be obtained from the Stokes parameters. While use of the linear Stokes parameters simplifies many calculations, presentation of data with the parameters η , P_C , and P often simplifies interpretation. In particular, η and P_C parameterize the polarization state of the polarized part of the beam, while P characterizes the unpolarized part. Furthermore, for many scattering mechanisms and experimental geometries, P_C is close to zero, so that η alone distinguishes amongst dominant scattering mechanisms, e.g., exposed and buried roughness.

The coherent source and high angular resolution of the instrument results in a large amount of speckle noise in intensity data, compared to instruments which use broad band sources. While the systematic sources of uncertainty are small (about 1 % of the signal at 95 % confidence level), the speckle noise dominates the uncertainties in the measurements. This source of uncertainty can be estimated by considering the apparent random point-to-point fluctuations in the measured data.

4. Results and Discussion

Figure 2 shows the calculated BRDF for unpolarized light incident with $\theta_i = 60^\circ$ for two exponential slope distribution functions [using Eq. (42) in Eq. (49), with $\sigma = 0.1$ and 0.2 and $C = 1$], respectively, and for different coating refractive indices (index $n = 1, 1.5,$ and 2). The index of refraction used for the substrate or flakes is that appropriate for aluminum ($n_f = 1.37 + 7.62i$).¹⁴ The case of $n = 1$ corresponds to the absence of any coating. For any given coating index, the wider the distribution of facet slopes, the wider the scattering distribution. As the scattering distribution widens, the near specular scattering decreases, and the large angle scattering increases. When the coating is included, and as the coating index is increased, the scattering distribution also broadens, but it does so in a manner which decreases the total integrated reflectance more than that observed for a broadened distribution without a coating. In Table 1, we show the integrated reflectance for unpolarized light calculated for the six conditions shown in Fig. 2, in addition to that predicted for $\sigma = 0.0$ (flat surface), and for a perfectly conducting substrate [$n_f \rightarrow \infty(1+i)$] and a silicon substrate ($n_f = 3.88 + 0.02i$).¹⁴ The total reflectance in the absence of a coating ($n = 1.0$) is always close to that for a flat surface, for the slope distributions studied. Additional loss of energy as the distribution widens results mostly from the small percentage of rays which are reflected into the substrate. As the coating index is increased on the metallic materials, additional loss of reflectance results from an increased reflectance from the exposed coating surface. As the distribution is widened with a coating, even more loss of reflectance occurs, since the spread of angles internal to the coating narrows with increased coating index and more light is lost to total internal reflection. Presumably, some of this loss of reflectance would be recovered if multiple scattering were included in the calculations, and would be expected to yield a diffuse scattering background. For the case of the silicon substrate an additional loss of reflectance is observed, which results from the partial matching of the coating-substrate indices and the concomitant lowering of the coating-substrate

reflectance. These results are in agreement with the general observation that coated surfaces tend to appear darker than uncoated surfaces. The higher the index of the coating, the darker the material and, since the reflectance of the coating increases, the glossier the material.

Figure 3 shows the results of measurements performed in the plane of incidence for $\theta_i = 60^\circ$. The sample consisted of an aluminum-flake pigmented coating with a clear coating applied on top. The coating and the flake binder consisted of an acrylic-melamine polymer. The BRDF, f_r , exhibits a large peak in the specular direction, and a slowly varying diffuse background. Since the detection aperture was fixed (about 0.7° full angle), the BRDF in the region of the specular beam represents an average over this solid angle. Data is excluded in the region from $\theta_r = -67^\circ$ to $\theta_r = -53^\circ$, due to obscuration of the incident beam by the receiver assembly. For the polarization parameters, model calculations assuming an index of refraction appropriate for aluminum ($n_f = 1.37 + 7.62i$) and a polymer coating ($n = 1.5$) are shown as solid curves, while those for a polymer substrate with no coating, representative of scattering from the exposed interface, are shown as dashed curves. Close to the specular direction, the measured polarization state agrees well with the model for scattering by roughness of the exposed coating surface. At larger scattering angles, the measured polarization state agrees well with the model for scattering by the aluminum flakes beneath the coating. While the model does not predict any depolarization, due to its lack of treatment of multiple scattering, significant depolarization is observed at large scattering angles. Dips in the degree of polarization on both sides of the specular direction are observed and occur due to the presence of two competing scattering sources, as one scattering source (surface roughness of the coating) decays and the other (the subsurface facets) begins to dominate. The agreement between the measured polarization state and that predicted by the model in different regimes supports the validity of the analysis of the reflectance factor described in Sec. 2.B and our assignment of the dominant scattering mechanisms.

Data were collected using the in-plane geometries as well as the out-of-plane geometries described in Sec. 3. Using data measured in a regime where the polarization indicates that the aluminum flakes dominate the scattering intensity, we used Eq. (49) for the BRDF to determine the distribution function of surface slopes. In this analysis, we ignored the depolarization observed in the measured data, and simply divided the measured BRDF by that predicted (per unit slope distribution) by the theory. Fig. 4 shows the results of this analysis. Evaluation of the integral given in Eq. (33) yields a normalization of 0.77, reasonably close to unity, given that the slope distribution is not measured to infinite slope, given the approximations made in the theory, and given that the coverage of the flakes may not be complete.

A significant observation in Fig. 4 is that the measured slope distribution function lies along a common curve, despite being measured in different geometries. While other measurements using confocal microscopy⁸ suggest that these results do not represent the distribution of flake orientations as much as they represent the local roughness of the flakes, the finding that the results lie along a single curve suggests that we have found scaling properties that enable single-scan measurements for fixed incident angle to predict the scattering in a wide variety of other geometries. Such scaling properties simplify the characterization of these materials for quality control applications and visual rendering. The finding that the data in Fig. 4 lies along a nearly straight line suggests that an exponential distribution function is appropriate for this sample.

5. Concluding Remarks

We have developed a model for light scattering by flake pigmented coatings and rough surfaces beneath smooth dielectric coatings. The results connect the distribution of the flake orientations or the local surface orientation distribution to the BRDF. Measurement results suggest that the model does a reasonable job of predicting the approximate light scattering properties of the sample, including the intensity distribution and the polarization. While we did not describe any results using interference coated metallic or dielectric flakes (pearlescent pigments), it is expected that the model will apply to some degree to these types of pigments as well, by using reflection and transmission coefficients appropriate for surfaces with thin films.¹⁵

Further refinements of this problem should be considered in the future. Multiple scattering was ignored in the present model but would be expected to contribute significantly to the scattering distribution, especially for cases where the flakes are transparent and there is significant stacking of flakes. The depolarization observed in the present measurements suggest that multiple scattering is important for these conditions as well. For pigment-saturated coatings, rays which are totally internally reflected by the coating would have a high probability of striking multiple flakes.

Lastly, it is expected that shadowing and obscuration will be important in many conditions. For example, if the surface is very rough, those surface facets which are directed away from the incident direction will shadow neighboring areas on the surface. Likewise, for flake pigments embedded in the coating in high enough concentrations to hide the underlying medium, it is expected that there will be flakes which overlap other flakes. While shadowing and obscuration has been analyzed for the case of a rough surface,^{7,16} we are unaware of work which has been performed which is specific for flake pigments.

Acknowledgements

The authors would like to thank Brent Laurenti of Eckart America for providing samples, and Lipiin Sung, Maria Nadal, and Mary McKnight for useful discussions.

Appendix

The Fresnel reflection coefficients, given an incident angle of θ , incident medium of index n_1 , and transmitting medium of index n_2 , for an interface without any interference films are

$$r_s(\theta; n_1, n_2) = \frac{\cos \theta - [(n_2/n_1)^2 - \sin^2 \theta]^{1/2}}{\cos \theta + [(n_2/n_1)^2 - \sin^2 \theta]^{1/2}}, \quad (\text{A.1})$$

$$r_p(\theta; n_1, n_2) = \frac{(n_2/n_1) \cos \theta - [(n_2/n_1)^2 - \sin^2 \theta]^{1/2}}{(n_2/n_1) \cos \theta + [(n_2/n_1)^2 - \sin^2 \theta]^{1/2}} \quad (\text{A.2})$$

for s and p polarized light, respectively. The transmission coefficients are

$$t_s(\theta; n_1, n_2) = \frac{2n_1 \cos \theta}{\cos \theta + [(n_2/n_1)^2 - \sin^2 \theta]^{1/2}}, \quad (\text{A.3})$$

$$t_p(\theta; n_1, n_2) = \frac{2(n_1/n_2)\cos\theta}{(n_2/n_1)\cos\theta + [(n_2/n_1)^2 - \sin^2\theta]^{1/2}}. \quad (\text{A.4})$$

References

1. R. Glausch, M. Kieser, R. Maisch, G. Pfaff, and J. Weitzel, *Special Effect Pigments*, (Vincentz Verlag, Hannover, 1998).
2. G. Pfaff and P. Reynders, "Angle-dependent optical effects deriving from submicron structures of films and pigments," *Chem. Rev.* **99**, 1963-1981 (1999).
3. F.E. Nicodemus, J.C. Richmond, J.J. Hsia, I.W. Ginsberg, and T. Limperis, *Geometrical Considerations and Nomenclature for Reflectance*, (National Bureau of Standards, Gaithersburg, 1977).
4. J.C. Stover, *Optical Scattering: Measurement and Analysis*, (SPIE Optical Engineering Press, Bellingham, WA, 1995).
5. D.E. Barrick, "Rough surface scattering based on the specular point theory," *IEEE Trans. Ant. Prop* **AP-16**, 449-454 (1968).
6. D.O. Muhleman, "Radar Scattering from Venus and the Moon," *The Astronomical Journal* **69**, 34-41 (1964).
7. K.E. Torrance and E.M. Sparrow, "Theory of off-specular reflection from roughened surfaces," *J. Opt. Soc. Am.* **57**, 1105-1114 (1967).
8. L. Sung, M.E. Nadal, M.E. McKnight, E. Marx, and B. Laurenti, "Optical reflectance of metallic coatings: Effect of aluminum flake orientation," *J. Coatings Tech.* **74**, 55-63 (2002).
9. M.E. McKnight, T.V. Vorburger, E. Marx, M.E. Nadal, P.Y. Barnes, and M.A. Galler, "Measurements and predictions of light scattering from clear coatings," *Appl. Opt.* **40**, 2159-2168 (2001).
10. M. Born and E. Wolf, *Principles of Optics*, (Pergamon, Oxford, 1980).
11. T.A. Germer and C.C. Asmail, "A goniometric optical scatter instrument for bidirectional reflectance distribution function measurements with out-of-plane and polarimetry capabilities," in *Scattering and Surface Roughness*, Z.-H.Gu and A.A.Maradudin, Eds., *Proc. SPIE* **3141**, 220-231, (1997).
12. T.A. Germer and C.C. Asmail, "Goniometric optical scatter instrument for out-of-plane ellipsometry measurements," *Rev. Sci. Instr.* **70**, 3688-3695 (1999).
13. T.A. Germer, "Polarized light scattering by microroughness and small defects in dielectric layers," *J. Opt. Soc. Am. A* **18**, 1279-1288 (2001).
14. E.D. Palik, *Handbook of Optical Constants of Solids*, (Academic, San Diego, 1985).
15. T.A. Germer and M.E. Nadal, "Modeling the appearance of special effect pigment coatings," in *Surface Scattering and Diffraction for Advanced Metrology*, Z.-H.Gu and A.A.Maradudin, Eds., *Proc. SPIE* **4447**, 77-86, (2001).
16. B.G. Smith, "Geometrical Shadowing of a Random Rough Surface," *IEEE Trans. Ant. Prop* **AP-15**, 668-671 (1967).

Table I. Total integrated reflectance of the coating on rough perfectly conducting, aluminum, and silicon surfaces for different exponential slope distribution functions and coating indices. Only scattering by the rough surface, and not the coating surface, is included in the reflectance.

Substrate	Coating index, n	$\sigma=$	$\sigma=$	$\sigma=$
		0.0	0.1	0.2
Perfect Conductor	1.0	1.00	1.00	0.98
	1.5	0.83	0.67	0.55
	2.0	0.71	0.51	0.39
Aluminum	1.0	0.90	0.89	0.88
	1.5	0.73	0.58	0.48
	2.0	0.61	0.42	0.33
Silicon	1.0	0.35	0.35	0.34
	1.5	0.15	0.12	0.10
	2.0	0.07	0.05	0.04

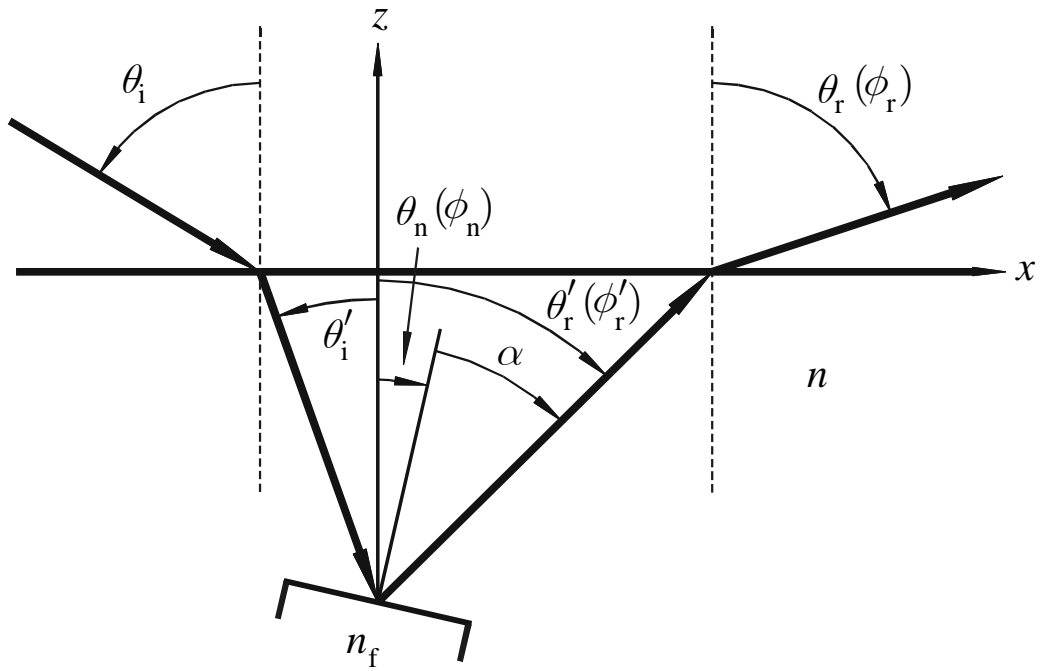


Figure 1. The ray trajectory for an oblique surface element. Azimuthal angles associated with directions are shown in parentheses.

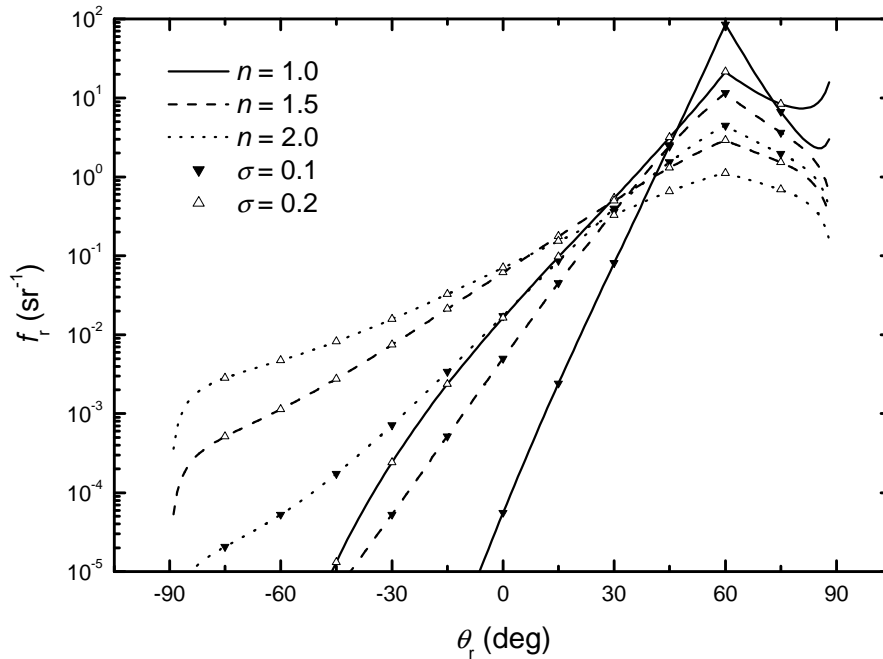


Figure 2. Calculated BRDF for different slope distribution functions, characterized by rms slope σ , and coating index n . The incident angle was $\theta_i = 60^\circ$, the substrate was aluminum, and the wavelength was 633 nm.

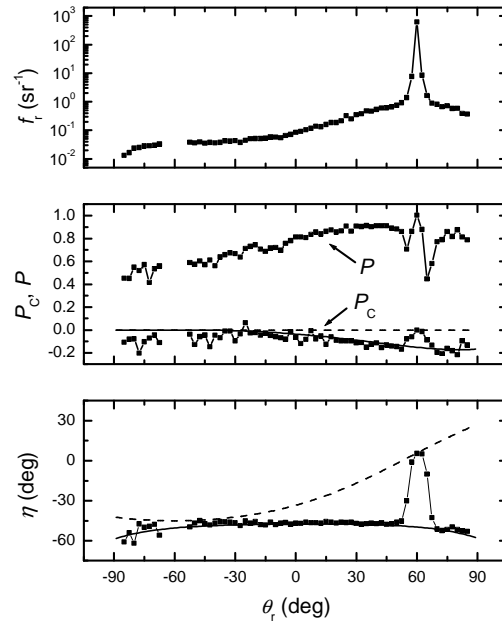


Figure 3. Data measured from an aluminum flake pigment under a smooth coating. The light was incident at an angle of $\theta_i = 60^\circ$ and polarized 45° from the plane of incidence, and the wavelength was 633 nm. The top frame shows the BRDF, the middle frame shows the degree of polarization and degree of circular polarization, and the bottom frame shows the principal angle of polarization.

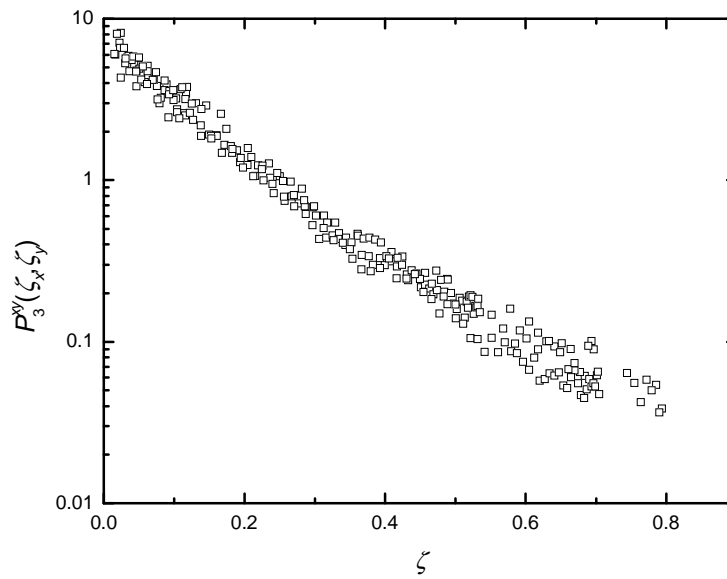


Figure 4. The slope distribution function derived from the data shown in Fig. 3.